

Improved reset breakdown strength in a HfO_x -based resistive memory by introducing RuO_x oxygen diffusion barrier

Cite as: AIP Advances 6, 055114 (2016); <https://doi.org/10.1063/1.4950966>

Submitted: 22 December 2015 . Accepted: 09 May 2016 . Published Online: 16 May 2016

Jaesung Park , Jiyong Woo, Amit Prakash, Sangheon Lee, Seokjae Lim, and Hyunsang Hwang



View Online



Export Citation



CrossMark

ARTICLES YOU MAY BE INTERESTED IN

[Oxygen migration during resistance switching and failure of hafnium oxide memristors](#)

Applied Physics Letters **110**, 103503 (2017); <https://doi.org/10.1063/1.4974535>

[Threshold switching behavior of Ag-Si based selector device and hydrogen doping effect on its characteristics](#)

AIP Advances **5**, 127221 (2015); <https://doi.org/10.1063/1.4938548>

[Conduction mechanism of TiN/ \$\text{HfO}_x\$ /Pt resistive switching memory: A trap-assisted-tunneling model](#)

Applied Physics Letters **99**, 063507 (2011); <https://doi.org/10.1063/1.3624472>

AVS Quantum Science

Co-published with AIP Publishing



Coming Soon!

Improved reset breakdown strength in a HfO_x-based resistive memory by introducing RuO_x oxygen diffusion barrier

Jaesung Park, Jiyong Woo, Amit Prakash, Sangheon Lee, Seokjae Lim, and Hyunsang Hwang^a

Department of Materials Science and Engineering, Pohang University of Science and Technology, Pohang, 790-784, Republic of Korea

(Received 22 December 2015; accepted 9 May 2016; published online 16 May 2016)

We investigated the reset breakdown phenomenon of HfO_x-based resistive memory for reliable switching operation in a fully CMOS compatible stack. Through the understanding on the effect of electrode materials and device area, our findings show that observed failure is attributed to additional oxygen vacancies close to the electrode interface, where switching is occurred. Therefore, RuO_x serving as an oxygen diffusion barrier was introduced to suppress the generation of unwanted oxygen vacancies by preventing out-diffusion of oxygen through the electrode. As a result, significantly enhanced breakdown strength in HfO_x/RuO_x stack is achieved and resulting in improved cycle endurance with larger on/off ratio. © 2016 Author(s). All article content, except where otherwise noted, is licensed under a Creative Commons Attribution (CC BY) license (<http://creativecommons.org/licenses/by/4.0/>). [<http://dx.doi.org/10.1063/1.4950966>]

INTRODUCTION

Resistive random-access memory (RRAM) has been considered as one of the promising candidates for NAND FLASH memory because of the low power operation (~ pJ), high scalability (sub-10 nm), and CMOS compatibility.^{1,2} These attractive characteristics of RRAM are attributed to the physical mechanism, which has been known as the redox reaction of oxygen vacancy in various transition-metal oxides including TiO₂, Ta₂O₅ and HfO₂.²⁻⁹ Owing to the transition between formation and rupture of a filament at oxide/electrode interface, low-resistance state (LRS) and high-resistance state (HRS) can be reversibly obtained.

Although, the use of localized filament accompanying the migration of oxygen vacancies in RRAM is beneficial to the switching characteristics, stochastic movement of oxygen vacancies causes performance degradation in reliability test such as data retention, switching uniformity, and cycling endurance.^{10,11} Not only that, it has been recently reported that unexpected permanent breakdown was induced when the device was switched from LRS to HRS i.e. during the reset process.^{12,13} After the breakdown, the device stuck in LRS and further resistance switching could not be obtained. Based on the literature, this failure could be contributed by the amount of oxygen vacancies at the bottom electrode (BE), which was not involved in switching operation. However, the effect of BE conditions on the breakdown behavior has not yet been fully understood.

Therefore, in this study, the reset breakdown phenomenon in HfO_x-based RRAM was systematically investigated by considering the reactivity of BE materials and the size of active device area. Our result revealed that the device failure with low breakdown voltage was mainly observed when the considerable amount of oxygen vacancies at HfO_x/BE interface were induced. Hence, RuO_x layer serving as an oxygen diffusion barrier was inserted into BE interface to minimize the

^aCorresponding Author E-mail Address: hwanghs@postech.ac.kr

formation of unwanted oxygen vacancies, and the reliable switching characteristics with enhanced breakdown strength were achieved.

EXPERIMENTAL PROCEDURES

The HfO_x-based RRAM device was fabricated on W-substrate with various device diameters of 200 nm, 500 nm, 700 nm, and 1 μm. A 4 nm-thick HfO_x switching layer was deposited by atomic layer deposition (ALD) technique at 250 °C. For comparison of effect of electrodes, 100-nm-thick films of various materials of Pt, Ru, and Ta were deposited by using sputtering system at room temperature. For the deposition of 60-nm-thick RuO_x layer, reactive sputtering was used with Ru metal target in an Ar (30 sccm) and O₂ (3 sccm) ambient.

RESULTS & DISCUSSION

Note that we intentionally applied positive bias on the W-substrate to clarify the effect of BE on the breakdown behavior. Thus, the TE was fixed as W-substrate, and various electrode materials can be evaluated as BE hereafter, as shown in inset of Fig. 1(a). The switching current in all the samples were identically limited at 300 μA to prevent the damage into the cells due to overflowing current. Fig. 1(a) shows the typical I-V characteristics of W/HfO_x/BE stack with 1 μm² active area. It is obvious that the typical resistive switching characteristics were observed irrespective of the BE materials, while the breakdown behavior was only occurred in the Ta BE device during reset process close to the reset voltage. To understand the relation between BE and breakdown behavior, we extracted breakdown voltage (V_{BD}) from the DC I-V data with increased stop voltage, as shown in Fig. 1(b). The current gradually decreased by applying RESET voltage, and then sudden increase in the current was observed at higher voltage regime. The average value of V_{BD} as a function of BE materials clearly indicate that the higher the oxygen affinity of BE, the smaller is the V_{BD} . This V_{BD} trend can be understood by considering Gibbs free energy (ΔG) of formation of oxide, which is

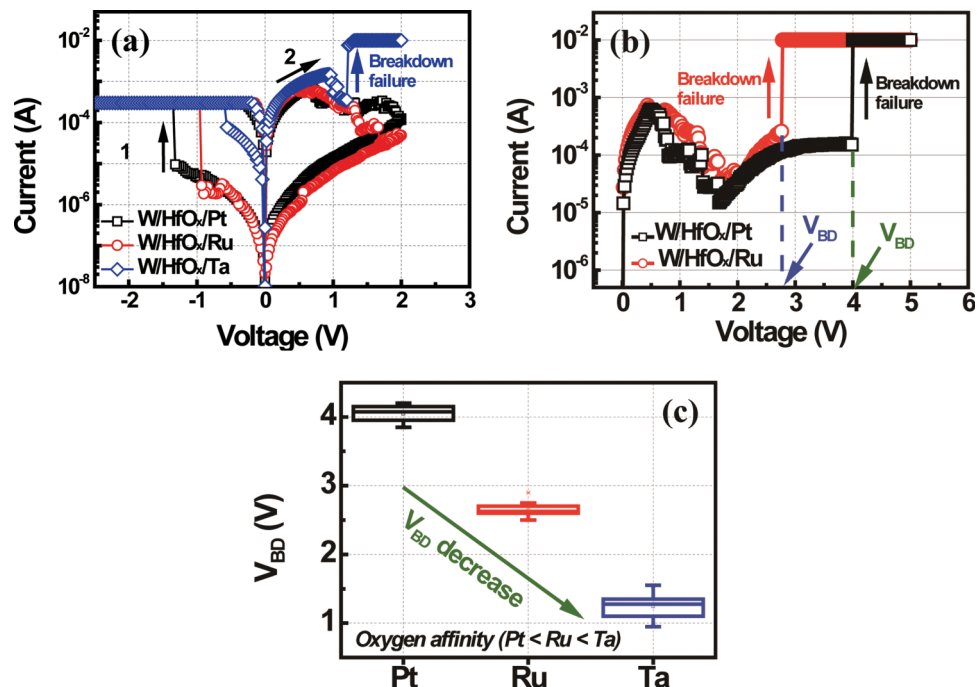


FIG. 1. (a) The I-V characteristics of W/HfO_x/Pt (Pt BE), W/HfO_x/Ru (Ru BE), and W/HfO_x/Ta (Ta BE) devices after forming process. In Ta BE device, the breakdown failure is shown in 1.2V. (b) The breakdown voltage (V_{BD}) of Pt BE and Ru BE device. (c) Distribution of V_{BD} values in each device.

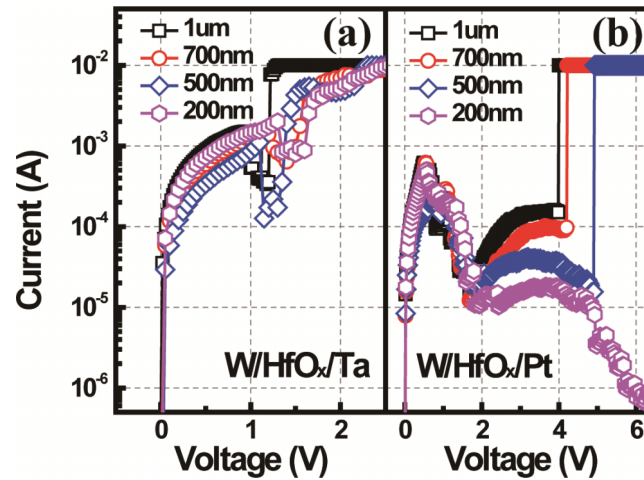


FIG. 2. Measurement of V_{BD} with device area in (a) Ta BE device, (b) Pt BE device. The V_{BD} is increased with decrease of device area in Pt BE device.

generally represented as the index of redox reaction.¹⁴ The lower absolute value of ΔG value favors lower redox reaction at electrode/oxide interface. Therefore, the Ta electrode which has ΔG value of -760 kJ/mol can absorb more oxygen than that of Ru and Pt electrodes which have ΔG values of -213 kJ/mol and -164 kJ/mol respectively.^{15–17} This means that a lot of oxygen vacancies can be easily generated in Ta BE compared to Pt and Ru BE.

The lower V_{BD} obtained in the device having a large amount of oxygen vacancies close to BE was further verified by examining the effect of the device area on the V_{BD} as shown in Fig. 2(a) and 2(b). For the device with reactive Ta BE, breakdown around 1.5 V was observed regardless of active area. On the other hand, when active area was reduced from 1 μm to 200 nm for inert Pt BE, the V_{BD} was increased with respect to area scaling.

Based on these results, a plausible model can be proposed to explain the varying V_{BD} with respect to the reactivity of BE materials and device area, as shown in Fig. 3. It is generally explained that oxygen vacancies involved in the switching operation are mainly generated from reactive TE/oxide interface. The formed oxygen vacancies can be thus migrated towards bottom electrode

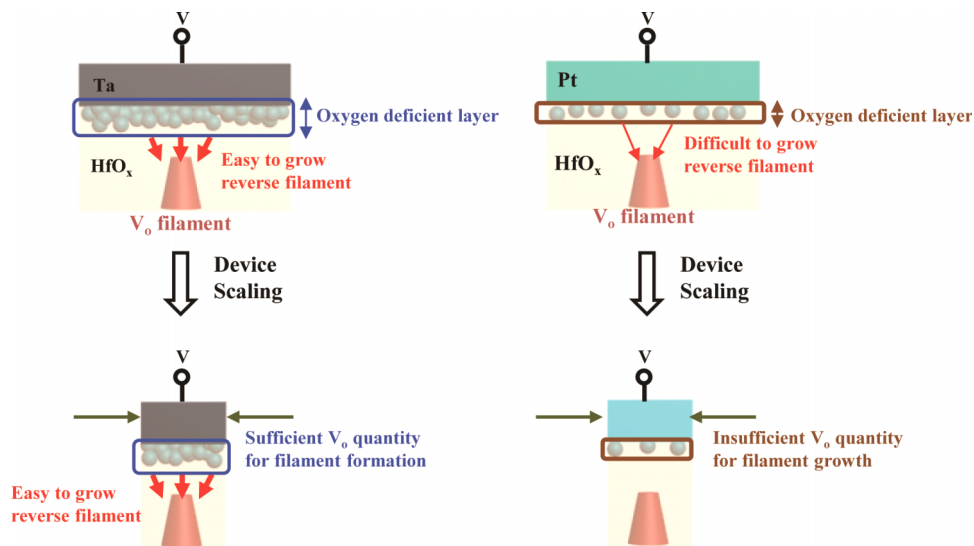


FIG. 3. The schematic diagram of breakdown failure process Ta BE device (left) and Pt BE device (right).

(BE) when we apply positive bias at TE, and then these vacancies form a conductive filament inside the oxide switching layer, which corresponds to LRS. On the other hand, the HRS can be achieved by drifting the oxygen vacancies apart from the filament close to BE under the smaller negative bias. It is worthy to note that this working scenario has been explained in case of a RRAM device having inert BE material such as Pt. When the RRAM device was fabricated on top of non-inert BE such as TiN, it should be considered for the generation of additional oxygen vacancies from the BE interface also.^{12,13} Thus, when the oxygen vacancies start to move away from the filament under the larger negative bias, additionally formed oxygen vacancies nearby BE simultaneously can move toward the ruptured regime. This re-connection of the filament in the HRS was the reason why the breakdown behavior was more easily observed in the reactive BE materials. In addition, when the active area was smaller, the probability of the generation of oxygen vacancies was decreased. Thus, the breakdown strength in the inert BE with a smaller active area was further enhanced, as shown in Fig 2(b). Based on the above results, inert metal electrode such as Pt should be considered to prevent the breakdown failure during reset operation due to the low oxygen vacancy quantity. However, the inert materials cannot be utilized in CMOS process because of etching and cost issues. While the tuning of bias conditions by applying small reset bias can also be used as an alternative approach, but it causes degraded switching on/off ratio.

Here, we suggested that the RuO_x layer was introduced to suppress the effect of scavenging on top of the HfO_x layer for fully CMOS compatible stack. The RuO_x material is widely used as an oxygen diffusion barrier to prevent the out-diffusion of oxygen through the electrode in ferroelectric memory application.^{18,19} The I-V characteristic of the $\text{HfO}_x/\text{RuO}_x$ system with 200nm device is shown in Fig. 4(a). The stable switching and high on/off ratio was obtained after 100 dc consecutive cycles. To confirm the breakdown phenomenon, the dc voltage sweep was conducted from 0V to 5V. The result is that the breakdown did not occur even for >5 V bias and it was similar to that of

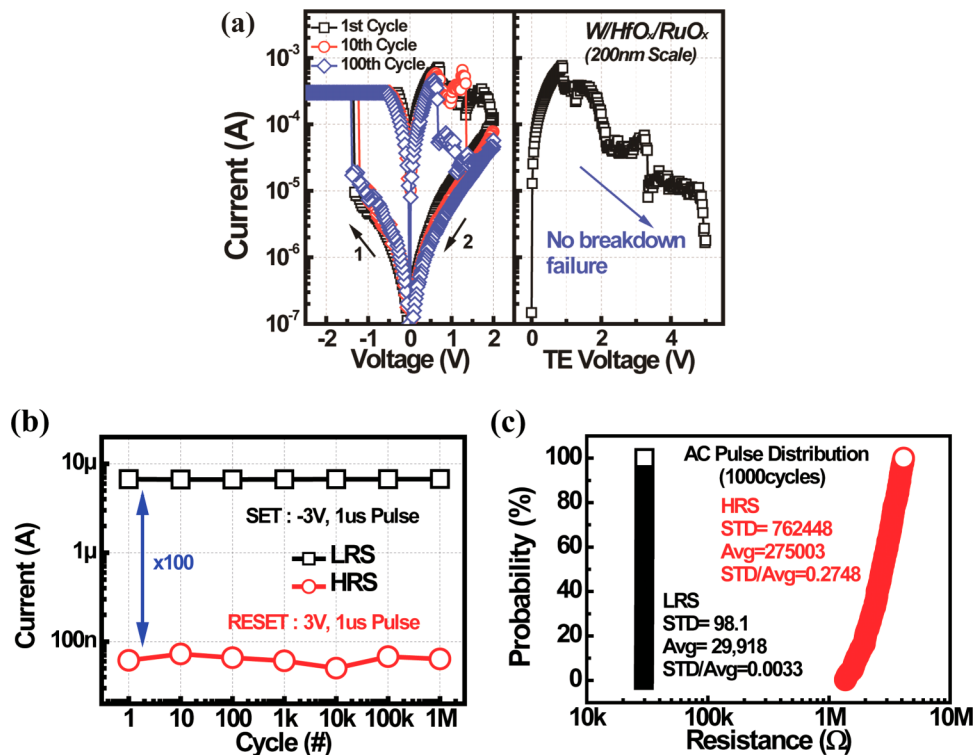


FIG. 4. (a) The I-V characteristic of the $\text{W}/\text{HfO}_x/\text{RuO}_x$ (RuO_x BE) device with 1, 10, and 100 cycles and evaluation of the breakdown failure of RuO_x BE device. The breakdown failure was not shown in RuO_x BE device. (b) AC pulse endurance and (c) the LRS and HRS resistance distribution of RuO_x BE device with 1us pulse width. The uniform resistance switching was obtained without the degradation of memory characteristic up to 10^6 .

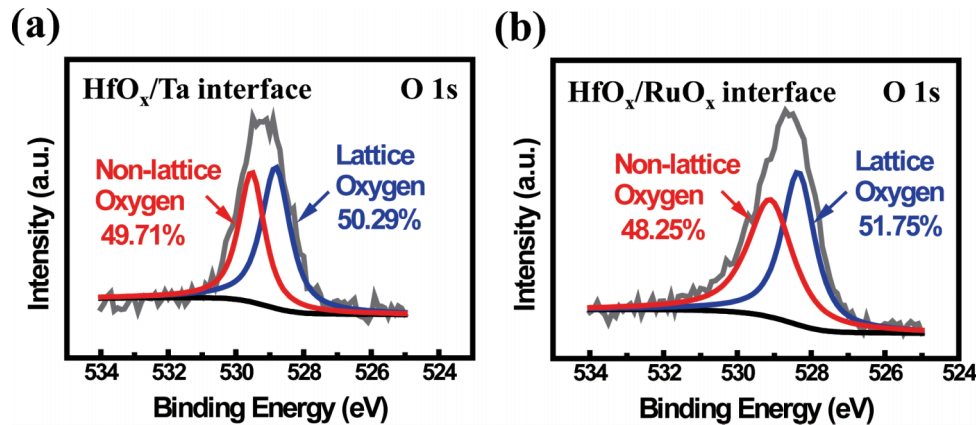


FIG. 5. Chemical bonding states of the O 1s states of (a) Ta BE device and (b) RuO_x BE at HfO_x/electrode interface.

the device with Pt BE. This observed robust switching behavior is beneficial not only for switching reliability but also for the possibility of multi-level cell due to the gradually increased resistance, which was controlled by the reset bias. Fig. 4(b) and 4(c) show the pulse endurance property of the RuO_x BE device. The pulse switching shows high memory margin of $>10^2$ and switching of $>10^6$ cycles with 1 μ s pulse width. In addition, the uniform 1000 consecutive switching cycle distribution was obtained as shown in Fig. 4(c).

We believed that this robust switching behavior was related to the restricted generation of oxygen vacancies by preventing the oxygen diffusion toward RuO_x from HfO_x. To analyze the oxygen state of the HfO_x/electrode interface, the X-ray photoelectron spectroscopy (XPS) was performed. Fig. 5(a) and 5(b) show the O 1s spectra of the HfO_x layer in Ta BE and RuO_x BE devices. According to the XPS result, the concentration of lattice oxygen is larger than the concentration of non-lattice oxygen in the RuO_x BE device. In contrast, the concentration of lattice oxygen is similar with the concentration of non-lattice oxygen in the HfO_x/Ta interface. The results indicated that the low oxygen vacancy quantity in the HfO_x/RuO_x interface.

CONCLUSION

In this study, the reset breakdown phenomenon in a HfO_x-based RRAM was investigated by means of various BE materials and device sizes. Our findings show that the large amount of oxygen vacancies at the BE interface, which could be generated by either scavenging effect of reactive electrode material or large active area, induced a permanent breakdown behavior. Thus, we introduced the RuO_x layer, serving as oxygen diffusion barrier, to minimize the formation of oxygen vacancies at the BE interface. This CMOS compatible HfO_x/RuO_x system allows the dramatically enhanced breakdown strength with robust switching characteristics.

ACKNOWLEDGEMENT

This research was supported by the Future Semiconductor Device Technology Development Program (10045226) funded by the Ministry of Trade, Industry, and Energy (MOTIE) and the Korea Semiconductor Research Consortium (KSRC) and supported by the Pioneer Research Center Program through the National Research Foundation of Korea funded by the Ministry of Science, ICT, and Future Planning (2012-0009460).

¹ L. Goux, A. Fantini, G. Kar, Y.-Y. Chen, N. Jossart, R. Degraeve, S. Clima, B. Govoreanu, G. Lorenzo, G. Poutois, D. J. Wouters, J. A. Kittl, L. Altimime, and M. Jurczak, VLSI Symp. Tech. Dig. 159–160 (2012).

² B. Govoreanu, G.S. Kar, Y.-Y. Chen, V. Paraschiv, S. Kubicek, A. Fantini, I.P. Radu, L. Goux, S. Clima, R. Degraeve, N. Jossart, O. Richard, T. Vandeweyer, K. Seo, P. Hendrickx, G. Pourtois, H. Bender, L. Altimime, D.J. Wouters, J.A. Kittl, and M. Jurczak, IEDM Tech. Dig. 729–732 (2011).

- ³ J. Joshua Yang, Matthew D. Pickett, Xuema Li, Douglas A. A. Ohlberg, Duncan R. Stewart, and R. Stanley Williams, *Nat. Nanotechnol.* **3**, 429 (2009).
- ⁴ Jubong Park, Seungjae Jung, Joonmyoung Lee, Wootae Lee, Seonghyun Kim, Jungho Shin, and Hyunsang Hwang, *Microelectron. Eng.* **88**, 1136 (2011).
- ⁵ Myoung-Jae Lee, Chang Bum Lee, Dongsoo Lee, Seung Ryul Lee, Man Chang, Ji Hyun Hur, Young-Bae Kim, Chang-Jung Kim, David H. Seo, Sunae Seo, U-In Chung, In-Kyeong Yoo, and Kinam Kim, *Nat. Mater.* **10**, 625 (2011).
- ⁶ Y. Hayakawa, A. Himeno, R. Yasuhara, W. Boullart, E. Vecchio, T. Vandeweyer, T. Witters, D. Crotti, M. Jurczak, S. Fujii, S. Ito, Y. Kawashima, Y. Ikeda, A. Kawahara, K. Kawai, Z. Wei, S. Muraoka, K. Shimakawa, T. Mikawa, and S. Yoneda, *VLSI Symp. Tech. Dig.* 14–15 (2015).
- ⁷ Soo Gil Kim, Tae Jung Ha, Seonghyun Kim, Jae Yeon Lee, Kyung Wan Kim, Jung Ho Shin, Yong Taek Park, Suk Pyo Song, Beom Yong Kim, Wan Gee Kim, Jong Chul Lee, Hyun Sun Lee, Jong Ho Song, Eung Rim Hwang, Sang Hoon Cho, Ja Chun Ku, Jong Il Kim, Kyu Sung Kim, Jong Hee Yoo, Hyo Jin Kim, Hoe Gwon Jung, Kee Jeung Lee, Suock Chung, Jong Ho Kang, Jung Hoon Lee, Hyeong Soo Kim, Sung Joo Hong, Gary Gibson, and Yoocham Jeon, *IEDM Tech. Dig.* 249–252 (2015).
- ⁸ Y. S. Chen, H. Y. Lee, P. S. Chen, C. H. Tsai, P. Y. Gu, T. Y. Wu, K. H. Tsai, S. S. Sheu, W. P. Lin, C. H. Lin, P. F. Chiu, W. S. Chen, F. T. Chen, C. Lien, and M.-J. Tsai, *IEDM Tech. Dig.* 717–719 (2010).
- ⁹ Joonmyoung Lee, Jungho Shin, Daeseok Lee, Wootae Lee, Seungjae Jung, Minseok Jo, Jubong Park, Kuyyadi P. Biju, Seonghyun Kim, Sangsu Park, and Hyunsang Hwang, *IEDM Tech. Dig.* 452–455 (2010).
- ¹⁰ Takeki Ninomiya, Shunsaku Muraoka, Zhiqiang Wei, Ryutaro Yasuhara, Koji Katayama, and Takeshi Takagi, *IEEE Electron Device Lett.* **35**, 214 (2013).
- ¹¹ Daeseok Lee, Jeonghwan Song, Jiyong Woo, Jaesung Park, Sangsu Park, Euijun Cha, Sangheon Lee, Yunmo Koo, Kibong Moon, and Hyunsang Hwang, *IEEE Electron Device Lett.* **34**, 762 (2014).
- ¹² C. Y. Chen, L. Goux, A. Fantini, S. Clima, R. Degraeve, A. Redolfi, Y. Y. Chen, G. Groeseneken, and M. Jurczak, *Appl. Phys. Lett.* **106**, 053501 (2015).
- ¹³ S. Balatti, S. Ambrogio, Z. Wang, S. Sills, A. Calderoni, N. Ramaswamy, and D. Ielmini, *IEEE Trans. Electron Devices* **62**, 3365 (2015).
- ¹⁴ Z. Wei, Y. Kanzawa, K. Arita, Y. Katoh, K. Kawai, S. Muraoka, S. Mitani, S. Fujii, K. Katayama, M. Iijima, T. Mikawa, T. Ninomiya, R. Miyayaga, Y. Kawashima, K. Tsuji, A. Himeno, T. Okada, R. Azuma, K. Shimakawa, H. Sugaya, T. Takagi, R. Yasuhara, K. Horiba, H. Kumigashira, and M. Oshima, *IEDM Tech. Dig.* 1–4 (2008).
- ¹⁵ L. Goux, A. Fantini, Y. Y. Chen, A. Redolfi, R. Degraeve, and M. Jurczak, *ECS Solid State Lett.* **11**, 79 (2014).
- ¹⁶ Yuichi MATSUI, Masahiko HIRATANI, and Shinichiro KIMURA, *Japan J. Appl. Phys.* **39**, 256 Number 1 (2000).
- ¹⁷ Joonmyoung Lee, El Mostafa Bourim, Wootae Lee, Jubong Park, Minseok Jo, Seungjae Jung, Jungho Shin, and Hyunsang Hwang, *Appl. Phys. Lett.* **97**, 172105 (2010).
- ¹⁸ A. Gruverman, O. Auciello, and H. Tokumoto, *Appl. Phys. Lett.* **69**, 3191 (1996).
- ¹⁹ Y. C. Choi and B. S. Lee, *Japan J. Appl. Phys.* **38**, 4876 Number 8 (1999).